

Orientation Angles of a Pulsar's Polarization Vector

Mark M. McKinnon

National Radio Astronomy Observatory,¹ Socorro, NM 87801 USA

ABSTRACT

A statistical model of the polarization of pulsar radio emission is used to derive the general statistics of a polarization vector's orientation angles. The theoretical distributions are compared with orientation angle histograms computed from single-pulse, polarization observations of PSR B2020+28. The favorable agreement between the theoretical and measured distributions lends support to the underlying assumptions of the statistical model, and demonstrates, like recent work on other pulsars, that the handedness of circular polarization is associated with the radiation's orthogonally polarized modes. Comprehensive directional statistics of the vector's orientation angles are also derived, and are shown to follow the Watson bipolar and Fisher distributions in its limiting forms.

Subject headings: methods: data analysis, statistical – polarization – pulsars: general – pulsars: individual (PSR B2020+28)

1. INTRODUCTION

Apart from the classic sweep of the polarization position angle across a pulsar's average profile, the orthogonal polarization modes (OPM) are perhaps the most striking feature in the polarization of pulsar radio emission. The modes appear in bimodal histograms of polarization position angle as two concentrations of data points separated by about 90° (e.g. Stinebring et al. 1984). The modes are elliptically as well as orthogonally polarized, so that the polarization states of the modes reside at antipodal points on the Poincaré sphere (Cordes et al. 1978). OPM are thought to arise from wave propagation effects in the magnetized plasma above the pulsar's polar cap (e.g. Allen & Melrose 1982; Barnard & Arons 1986). The simultaneous interaction of the modes may be responsible for the depolarization of the emission at high radio frequency (Manchester et al. 1975; Morris et al. 1981).

¹The National Radio Astronomy Observatory is a facility of the National Science Foundation operated under cooperative agreement by Associated Universities, Inc.

The notion that OPM are elliptically polarized suggests that the emission’s linear and circular polarization should be analyzed together, instead of individually, for a proper interpretation of pulsar polarization measurements (McKinnon 2003; hereafter M03). Comprehensive methods have been developed recently for displaying and analysing the polarization data in this way. For example, Karastergiou et al. (2003) plotted the measured orientation angles of a pulsar’s polarization vector in a Hammer-Aitoff projection, confirming the association of circular polarization handedness with OPM in PSR B1133+16. Similarly, Edwards & Stappers (2004; hereafter ES04) displayed the vector’s orientation angles in a Lambert equal-area projection to document and explore the intriguing deviations from mode orthogonality in PSR B0329+54. They also showed that the circular polarization in the pulsar is generally consistent with an origin in elliptically polarized OPM. McKinnon & Stinebring (1998, 2000) developed a statistical model of superposed OPM that predicts that polarization measurements at a given pulse longitude should form a single, prolate ellipsoid in the three-dimensional space defined by the Stokes parameters Q, U, and V. The prediction is generally supported by the analyses conducted by McKinnon (2004; hereafter M04) and ES04, who independently developed eigenvalue techniques to quantify the dimensions and orientations of the ellipsoids. While the eigenvalue analyses and the projections of polarization vector angles are generally supportive of the superposed OPM hypothesis, it has yet to be demonstrated that the observed orientation angles are consistent with those predicted by the OPM statistical model. The statistics of the orientation angles derived in M03 are limited in their applicability, primarily because they are restricted to the specific case of OPM with equal polarization amplitudes.

The objectives of this paper are to derive a general distribution for a polarization vector’s orientation angles by expanding the work of M03 and to compare the theoretical distribution with the distributions of observed orientation angles. The derivation is presented in §2, and the comparison is made in §3. Conclusions are discussed in §4.

2. THEORETICAL DISTRIBUTIONS OF ORIENTATION ANGLES

The joint probability density of a polarization vector’s amplitude, colatitude, and longitude must be determined from the Stokes parameters to calculate the individual distributions of the orientation angles. From the statistical model of pulsar polarization (M03), the equations for the measured Stokes parameters are

$$Q = \sin \theta_o \cos \phi_o (X_1 - X_2) + X_{N,Q}, \quad (1)$$

$$U = \sin \theta_o \sin \phi_o (X_1 - X_2) + X_{N,U}, \quad (2)$$

$$V = \cos \theta_o (X_1 - X_2) + X_{N,V}. \quad (3)$$

The random variables X_1 and X_2 represent the amplitudes of the mode polarization vectors. They have means μ_1 and μ_2 and standard deviations σ_1 and σ_2 . In general, X_1 and X_2 can be correlated random variables, but they are assumed to be independent in what follows. The Gaussian random variable X_N accounts for the instrumental noise. It has a zero mean and a standard deviation σ_N . The fixed angles θ_o and ϕ_o are the colatitude and longitude, respectively, of the diagonal in the Poincaré sphere along which the fluctuations in pulsar-intrinsic polarization occur. The angles correspond to twice the ellipticity and twice the position angle, respectively, of the polarization vector (i.e. $\theta_o = 2\chi_o$ and $\phi_o = 2\psi_o$ in the nomenclature of ES04). As discussed in M04, the emission may contain additional components, such as randomly polarized radiation (RPR). For the purposes of this paper, these components are neglected, or alternatively, assumed to be absorbed in the X_N terms provided that their fluctuations are Gaussian with a zero mean and that their Q-U-V covariance matrix is a scaled identity matrix.

The basic shape of a data point cluster formed by the equations for the Stokes parameters is a prolate ellipsoid. The orientation of the ellipsoid's major axis is determined by θ_o and ϕ_o . To simplify the derivation of the joint probability density of a polarization vector's amplitude and orientation, it is convenient to specify $\theta_o = 0$ so that the ellipsoid is symmetric about the z-axis in a conventional Cartesian coordinate system. By virtue of this symmetry, the longitude of the polarization vector is uniformly distributed over the interval $0 \leq \phi < 2\pi$, and the longitude and colatitude distributions are statistically independent. Since the ellipsoid retains its shape on rotation, measured distributions of colatitude and longitude can be compared with the theoretical result by determining the orientation of the measured ellipsoid's major axis, rotating the Q-U-V data points that form the ellipsoid via matrix multiplication so that the major axis of the rotated ellipsoid is aligned with the z-axis, and computing histograms of the rotated values of colatitude and longitude.

When $\theta_o = 0$ and when the mode polarization amplitudes, X_1 and X_2 , are independent, Gaussian random variables, the joint probability density of the measured polarization vector's amplitude and orientation is

$$f(r, \theta, \phi) = \frac{r^2 \sin \theta}{\sigma_N^3 (2\pi)^{3/2}} \frac{1}{(1 + \rho^2)^{1/2}} \exp \left[\frac{-r^2(1 + \rho^2 \sin^2 \theta) + 2r\mu \cos \theta - \mu^2}{2\sigma_N^2(1 + \rho^2)} \right]. \quad (4)$$

The parameter $\mu = \mu_1 - \mu_2$ is the mean value of the pulsar intrinsic polarization, and the parameter $\rho = (\sigma_1^2 + \sigma_2^2)^{1/2} / \sigma_N$ is a measure of the intrinsic polarization fluctuations relative

to the instrumental noise. Following the procedure outlined in M03, the joint probability density can be used to find the distribution of the polarization vector's amplitude.

$$f(r) = \frac{r^2}{\sigma_N^3} \frac{1}{[2\pi(1 + \rho^2)]^{1/2}} \exp\left[-\frac{(\rho^2 r^2 + \mu^2)}{2\rho^2 \sigma_N^2}\right] \int_{\mu/r\rho^2-1}^{\mu/r\rho^2+1} \exp\left[\frac{\rho^2 r^2 x^2}{2(1 + \rho^2)\sigma_N^2}\right] dx \quad (5)$$

Similarly, the vector's colatitude distribution is

$$f(\theta) = \frac{\sin \theta}{2} \frac{(1 + \rho^2)}{(1 + \rho^2 \sin^2 \theta)^{3/2}} \left\{ \exp\left[-\frac{s^2 \sin^2 \theta}{2(1 + \rho^2 \sin^2 \theta)}\right] \left[1 + \operatorname{erf}\left(\frac{y}{\sqrt{2}}\right)\right] (1 + y^2) + y \sqrt{\frac{2}{\pi}} \exp\left[-\frac{s^2}{2(1 + \rho^2)}\right] \right\}, \quad (6)$$

where y is a function of ρ , s , and θ given by

$$y = \frac{s \cos \theta}{[(1 + \rho^2 \sin^2 \theta)(1 + \rho^2)]^{1/2}}. \quad (7)$$

The colatitude distribution is characterized by two free parameters; the signal-to-noise ratio in polarization, $s = \mu/\sigma_N$, and the mode fluctuation ratio, ρ . The distribution is shown in Figure 1 for different values of s and ρ . The distribution is distinctly bimodal for large values of ρ , and becomes more sharply peaked at large values of s . Equation 6 generalizes the case-specific colatitude distributions for $s = 0$ and $\rho = 0$ derived in M03.

The conditional density of the polarization vector's colatitude, or the colatitude density at a fixed value of the polarization amplitude, r_o , is

$$f(\theta|r_o) = 2\pi \frac{f(r_o, \theta, \phi)}{f(r_o)} = \frac{\sin \theta}{w(\kappa, \gamma)} \exp[\kappa(\gamma + \cos \theta)^2], \quad (8)$$

where $w(\kappa, \gamma)$ is a normalization factor given by

$$w(\kappa, \gamma) = \int_{\gamma-1}^{\gamma+1} \exp(\kappa x^2) dx. \quad (9)$$

The colatitude conditional density is characterized by two dimensionless quantities; a concentration parameter given by $\kappa = r_o^2 \rho^2 / 2(1 + \rho^2) \sigma_N^2$ and a symmetry parameter given by

$\gamma = \mu/r_o\rho^2$. Examples of the conditional density are shown in Figure 2. The peaks in the distribution narrow as κ increases. When $\gamma = 0$ (e.g. when $\mu = 0$), the conditional density becomes the Watson bipolar distribution (eqn. 38 of M03), which is always symmetric about $\theta = \pi/2$. As γ increases, the conditional density is dominated by the strong polarization mode and peaks at small values of θ . The parameters κ and γ are not entirely independent. For example, when $\rho \ll 1$, κ becomes small and γ becomes very large, and the conditional density becomes the Fisher distribution with a concentration parameter of $\kappa_f = 2\gamma\kappa \simeq \mu r_o/\sigma_N^2$ (see eqn. 37 of M03). Statistical treatments of directional data (e.g. Fisher et al. 1987) appear to consider the Watson and Fisher distributions as completely unrelated. However, the analysis presented here clearly shows that the two distributions are special cases of the more comprehensive conditional density given by equation 8.

Figure 1 shows that the peaks in the colatitude distribution do not occur at the poles of the Poincaré sphere. In fact, both the locations and the widths of the peaks depend upon the values of s and ρ . The distribution gives the illusion that the data points in the Q-U-V cluster form annuli around the poles. The illusion arises from the computation of the colatitude distribution, which does not preserve the density of data points in the cluster (see also the discussion of equal-area projections in ES04). The polar concentration of data points is retained in the distribution of $u = \cos\theta$, where the locations of the OPM peaks occur at $\theta = 0, \pi$ and only the widths of the peaks are affected by s and ρ . The distribution of u can be computed directly from the distribution of θ given by equation 6. The distribution is

$$f(u) = \frac{1}{2} \frac{(1 + \rho^2)}{[1 + \rho^2(1 - u^2)]^{3/2}} \left\{ \exp \left[-\frac{s^2(1 - u^2)}{2[1 + \rho^2(1 - u^2)]} \right] \left[1 + \operatorname{erf} \left(\frac{\bar{y}}{\sqrt{2}} \right) \right] (1 + \bar{y}^2) \right. \\ \left. + \bar{y} \sqrt{\frac{2}{\pi}} \exp \left[-\frac{s^2}{2(1 + \rho^2)} \right] \right\}, \quad (10)$$

where \bar{y} is given by

$$\bar{y} = \frac{su}{\{[1 + \rho^2(1 - u^2)](1 + \rho^2)\}^{1/2}}. \quad (11)$$

The conditional density of u can be derived from equation 8.

$$f(u|r_o) = \frac{\exp[\kappa(\gamma + u)^2]}{w(\kappa, \gamma)} \quad (12)$$

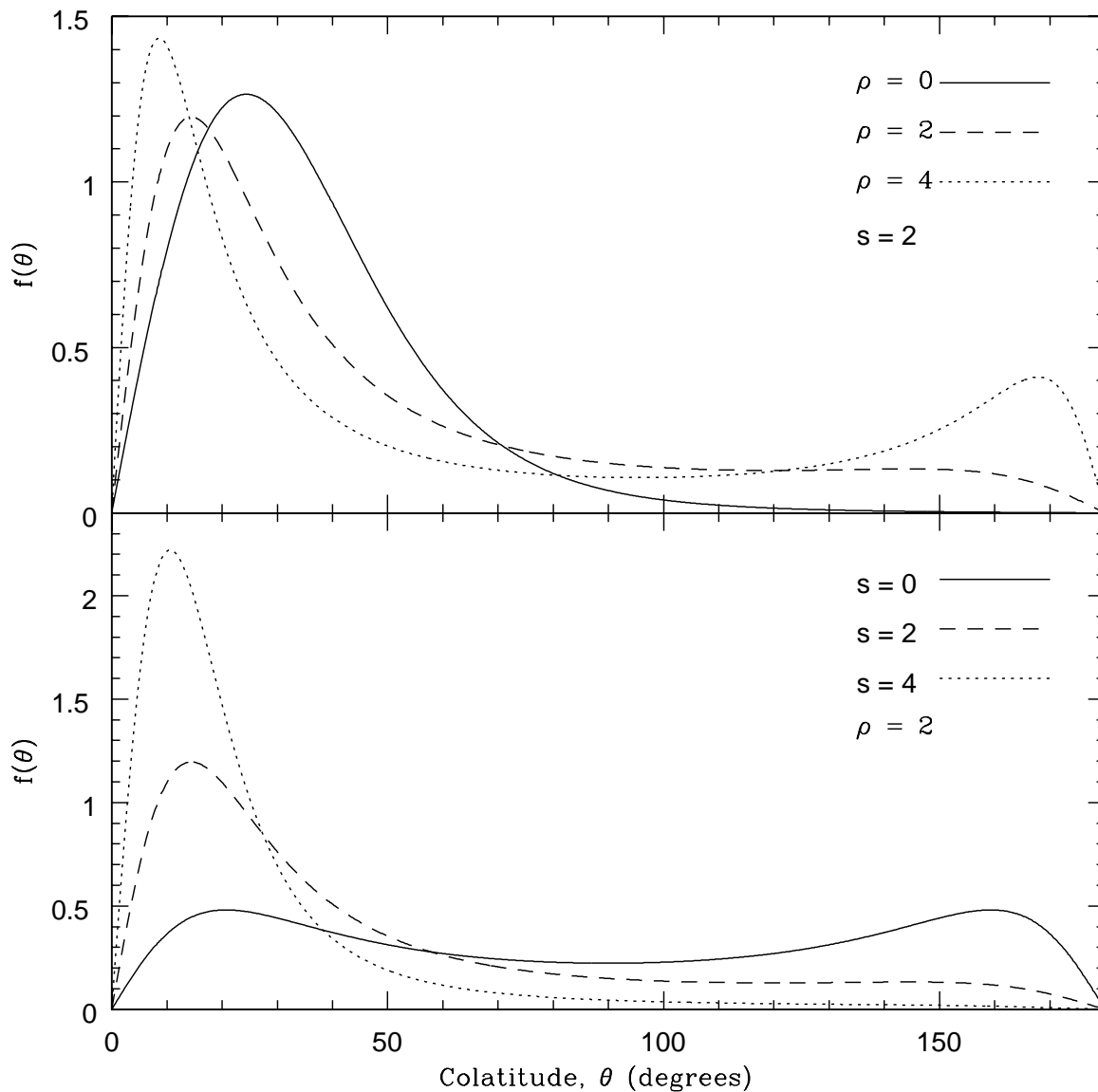


Fig. 1.— Distributions of a polarization vector’s colatitude, θ (eqn. 6). The top panel shows colatitude distributions for a fixed signal-to-noise ratio in polarization, s , with varying mode fluctuation ratio, ρ . The bottom panel shows colatitude distributions for fixed ρ and varying s .

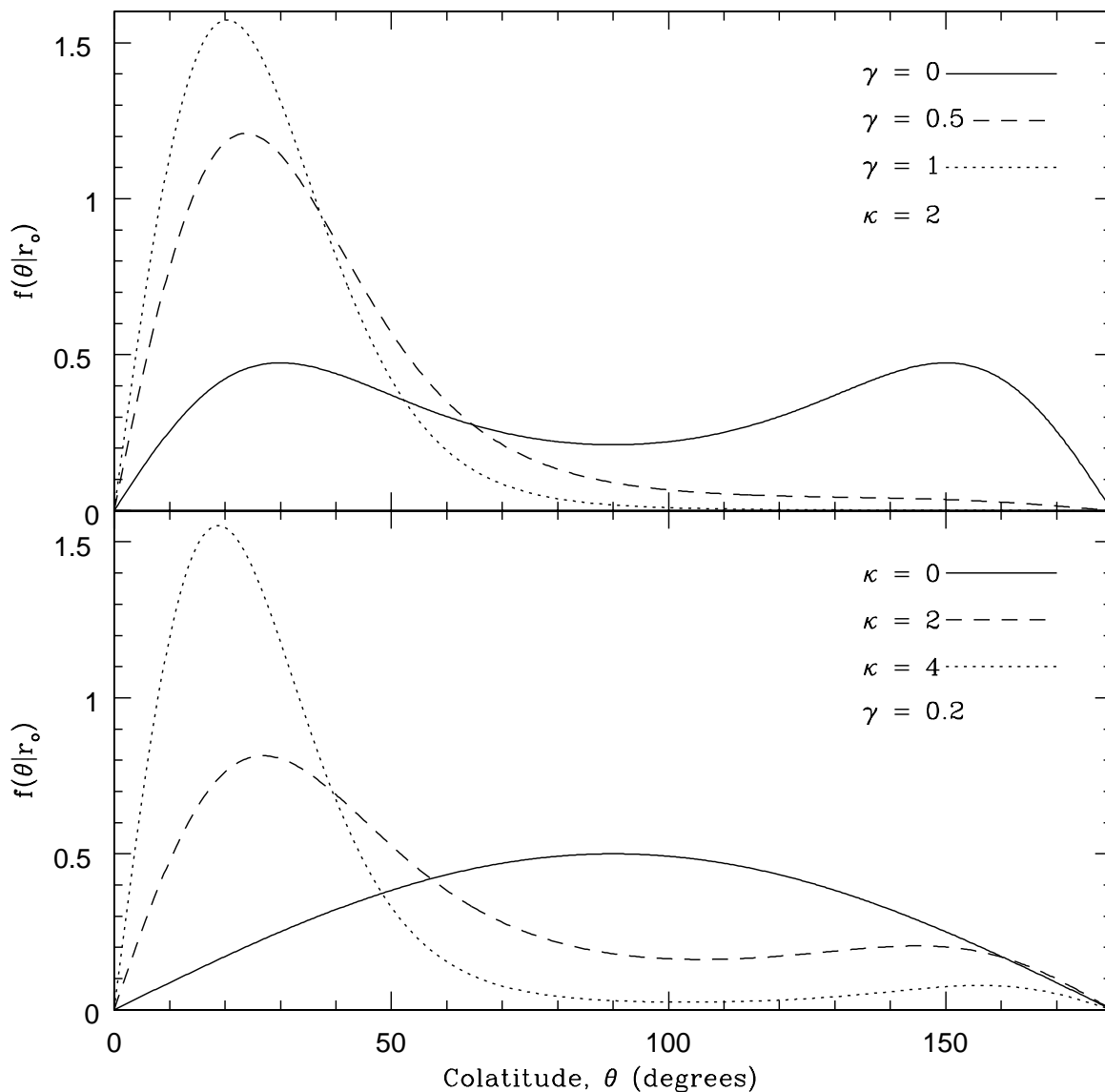


Fig. 2.— Conditional density of a polarization vector’s colatitude (eqn. 8). The distributions are shown for different concentration parameters, κ , and symmetry parameters, γ . The top panel shows distributions for varying γ with κ fixed. The bottom panel shows distributions for varying κ with γ fixed.

3. DISTRIBUTION COMPARISON

To compare the measured distributions of a polarization vector's colatitude and longitude with the analytical results, the Q-U-V data points comprising the polarization ellipsoid must be rotated so that the ellipsoid's major axis is aligned with the z-axis. From Fisher et al. (1987), the matrix multiplication operation that performs the rotation is

$$\begin{bmatrix} \cos \theta_o \cos \phi_o & \cos \theta_o \sin \phi_o & -\sin \theta_o \\ -\sin \phi_o & \cos \phi_o & 0 \\ \sin \theta_o \cos \phi_o & \sin \theta_o \sin \phi_o & \cos \theta_o \end{bmatrix} \begin{bmatrix} Q_o \\ U_o \\ V_o \end{bmatrix} = \begin{bmatrix} 0 \\ 0 \\ \mu \end{bmatrix}. \quad (13)$$

Care must be exercised in choosing appropriate estimates of the ellipsoid's orientation angles, θ_o and ϕ_o , before the rotation is performed. The angles could be estimated from the mean values of the Stokes parameters at the pulse longitude of interest from

$$\phi_o = \arctan\left(\frac{\langle U \rangle}{\langle Q \rangle}\right), \quad (14)$$

$$\theta_o = \arccos\left[\frac{\langle V \rangle}{(\langle Q \rangle^2 + \langle U \rangle^2 + \langle V \rangle^2)^{1/2}}\right], \quad (15)$$

which would suffice for locations within the pulse where the polarization signal-to-noise ratio is high, $s \gg 0$. But at locations where $s \simeq 0$, the mean Stokes parameters will be small, and consequently equations 14 and 15 will produce poor estimates of ϕ_o and θ_o . Alternatively, one could compute the covariances of the Stokes parameters, and the directional cosines of the principal eigenvector of the 3x3 covariance matrix could be used to estimate ϕ_o and θ_o . The polarization ellipsoid can be highly elongated where OPM occurs, and the directional cosines of the principal eigenvector can be well determined, even where $s = 0$, because its eigenvalue, $\tau_{11} = \sigma_N^2(1 + \rho^2)$ (M04), is a strong function of the mode fluctuation ratio, ρ . However, this method produces poor estimates of the orientation angles at locations where $\rho \simeq 0$, even if $s \gg 0$, because the eigenvalues in this case are equal ($\tau_{11} = \tau_{22} = \tau_{33} = \sigma_N^2$), and thus the eigenvectors are not unique. The best estimate of the ellipsoid's orientation angles, and the one used in the analysis presented below, comes from the directional cosines of the principal eigenvector determined from the second moments of the Stokes parameters. The eigenvalue of the second moment principal eigenvector is $\tau_{11} = \sigma_N^2(1 + s^2 + \rho^2)$, and the directional cosines of the eigenvector will be well determined when either $s \simeq 0$ or $\rho \simeq 0$. When both s and ρ are small, no polarized signal is present, the polarization ellipsoid is a spheroid centered on the origin of Q-U-V space, and there is no need to rotate the spheroid (i.e. the distribution of data points is isotropic).

Histograms of the measured values of colatitude and longitude were computed at different locations within the pulse of PSR B2020+28 using the 1404 MHz single pulse, polarization observations of Stinebring et al. (1984) as follows. From the multiple measurements of the Stokes parameters taken at each location, the second moments of the Stokes parameters were computed and used to find the directional cosines of the polarization ellipsoid’s principal eigenvector (major axis). The directional cosines were then used to compute the orientation angles of the major axis. The resulting values of θ_o and ϕ_o were used in equation 13 to rotate the Q-U-V data points that formed the polarization ellipsoid. Finally, the rotated Stokes parameters were used to calculate corresponding values of colatitude and longitude, which were binned into 50 intervals spread over the appropriate range of angles to form the histograms.

The histograms at three different locations in the pulse are compared with the theoretical distributions of the polarization vector’s colatitude and longitude in Figure 3. The colatitude distributions are shown in the left column of panels in the figure, and their corresponding longitude distributions are shown in the right column of panels. The solid horizontal line in each of the longitude histogram panels represents the uniform distribution expected from the OPM statistical model. The generally good agreement between the theoretical and measured longitude distributions, combined with the observation that the ratios of the minor axes of the Q-U-V data point clusters are no larger than 1.09 at these locations within the pulse (M04), suggests that the polarization ellipsoids are rotationally symmetric about their major axes. The observed symmetry of the ellipsoids also suggests that the longitude and colatitude of the polarization vector are statistically independent, as predicted by the OPM statistical model. However, the symmetry does not rule out the possibility that ϕ and θ can be correlated or dependent upon one another. Indeed, the deviations from orthogonality documented in ES04 and M04 are evidence that the two angles can be correlated. The smooth, solid curves shown in the colatitude histogram panels represent the best fits of the data to equation 6. The best fit values of ρ and s are annotated in each panel. The excellent fits show that equation 6 is capable of representing a broad range of polarization behavior. Furthermore, these fits and the measurements of cluster dimensions by M04 together imply that the clusters aren’t just any ellipsoids, but the ellipsoids expected from the OPM statistical model, suggesting quantitative, in addition to qualitative, consistency between the model and the data. The data used to construct the histograms had significant circular polarization, and the ellipsoidal shape of the Q-U-V data point clusters illustrates the association of circular polarization handedness with OPM in PSR 2020+28, similar to what was found in PSR 1133+16 by Karastergiou et al. (2003) and in PSR B0329+54 by ES04. Only one polarization mode is apparent ($\rho = 0$) in the colatitude histogram shown in the top left panel of the figure. In the lower panels, the other polarization mode becomes more obvious as indicated by the bimodal

histograms and the increasing value of ρ . Additionally, the values of s in the panels decrease as ρ increases, which is to be expected since the simultaneous interaction of the orthogonal modes depolarizes the emission. The fitted values of s are low when compared to what is expected from the mean polarization and the off-pulse instrumental noise. However, the sizes of the ellipsoids' minor axes, and thus the effective noise of the observations, are much larger than the off-pulse noise, causing the lower-than-expected values of s . An emission component such as RPR could contribute to the large effective noise (M04, ES04).

The measured and theoretical distributions of $\cos\theta$ are compared in Figure 4. The data shown in each panel of the figure are the same data used in the corresponding panel of the left column of Figure 3. The histogram in each panel is the measured distribution of $\cos\theta$. The smooth curve is the theoretical distribution computed from equation 10 using the same values of ρ and s as in Figure 3. In all panels, the data are concentrated at one or both of the poles. The agreement between the theoretical and measured distributions is excellent.

4. DISCUSSION AND CONCLUSIONS

The statistical model of pulsar polarization developed by McKinnon & Stinebring (1998) predicts that multiple measurements of the variable Stokes parameters at a fixed pulse longitude will form a single, prolate ellipsoid in Poincaré space. The analyses presented in ES04 and M04 show that Q-U-V data point clusters in PSR B0329+54, PSR B1929+10, and PSR B2020+28 are indeed prolate ellipsoids. In this paper, the favorable comparison between the theoretical and measured distributions of polarization vector colatitude and longitude in PSR B2020+28 suggest that the data point clusters are consistent with the ellipsoid expected from the model. This implies quantitative consistency between the model and the data, and supports the fundamental, underlying assumption of the statistical model which is the observed polarization is determined by the simultaneous interaction of two, orthogonally polarized modes.

The analysis of orientation angles presented here and the observations and analyses of Cordes et al. (1978), Karastergiou et al. (2003), and ES04 clearly demonstrate the association of circular polarization handedness with OPM, confirming that the modes are elliptically polarized and occupy antipodal points on the Poincaré sphere. This result could be interpreted to conclude that the circular polarization is formed by the appropriate phasing of the naturally occurring, linearly polarized modes through mode coupling (e.g. Lyubarskii & Petrova 1998; Petrova 2001) as the radiation propagates through the pulsar's magnetospheric plasma. If this were the case, we would only observe circular polarization in parts of the pulse where both modes were found. However, there are clear examples of circular

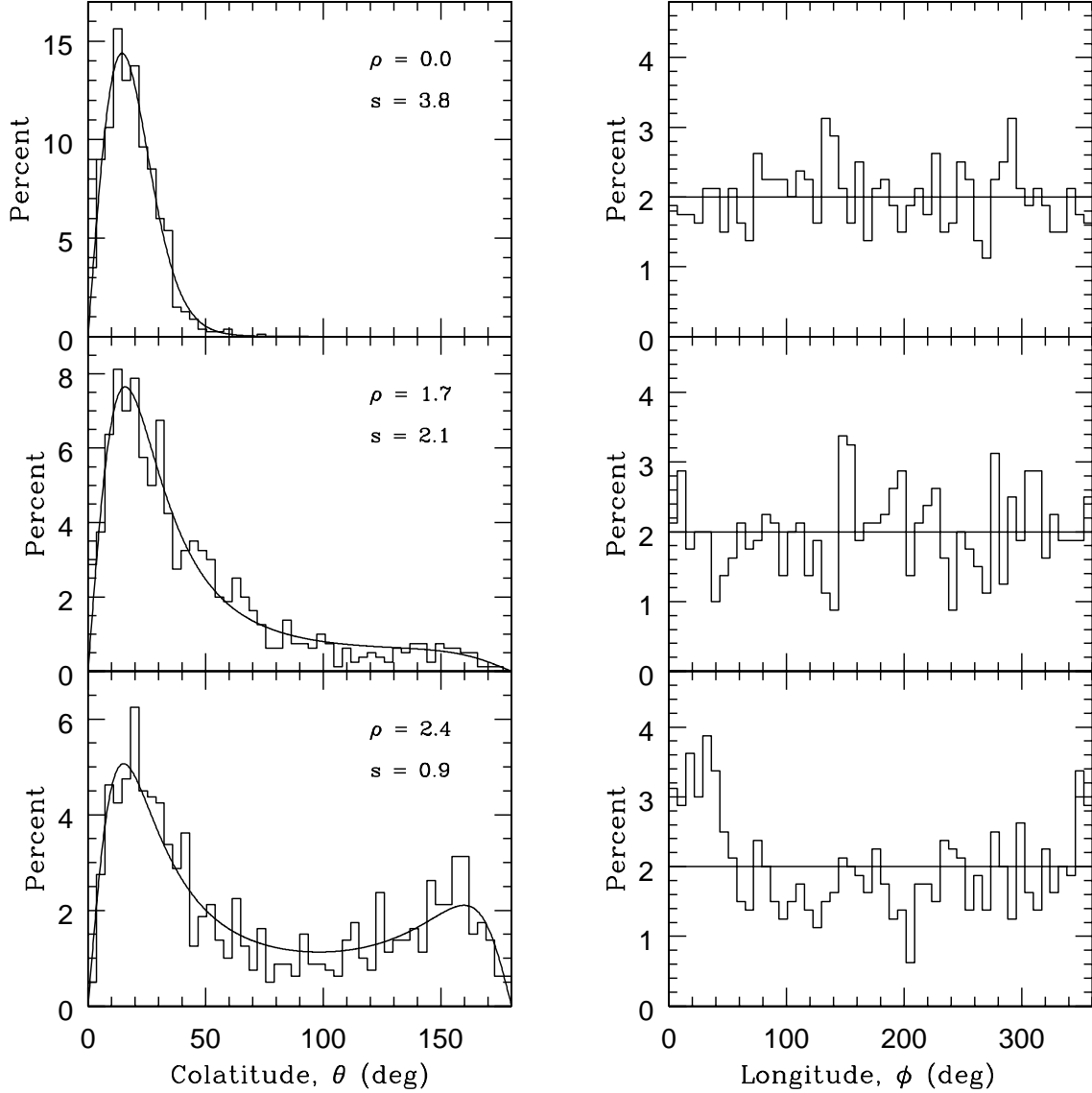


Fig. 3.— Comparison between the measured and theoretical distributions of a polarization vector’s colatitude and longitude at three different locations in the pulse of PSR B2020+28. The longitude histograms are generally consistent with the uniform distributions predicted by the statistical OPM model, as indicated by the solid horizontal line. The smooth curves through the colatitude histograms are best fits to equation 6. The fitted values of signal-to-noise ratio, s , and mode fluctuation ratio, ρ , are annotated in each colatitude histogram panel.

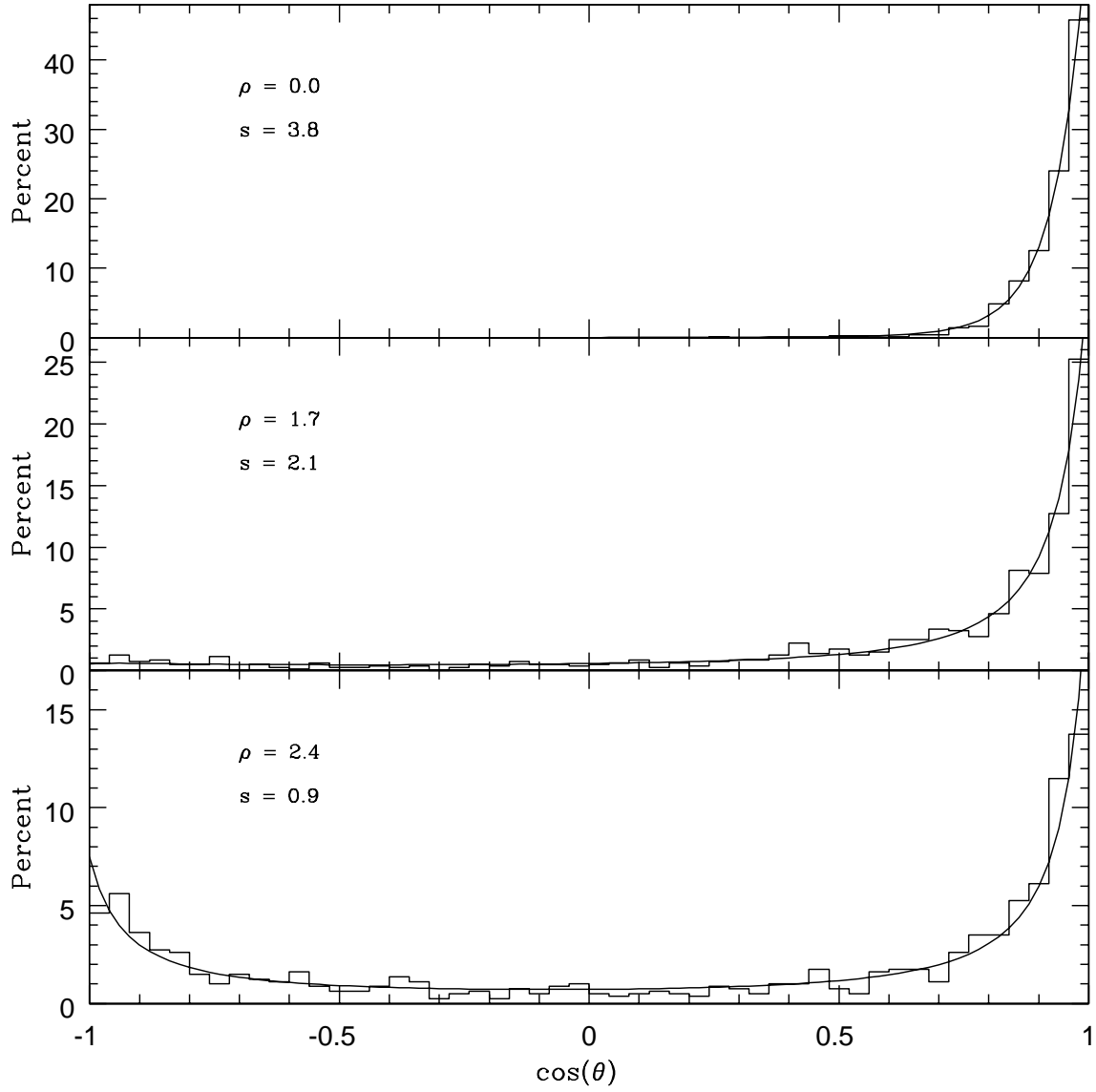


Fig. 4.— Comparison between the measured and theoretical distributions of cosine colatitude, $\cos \theta$, at the three locations in PSR B2020+28.

polarization where only one mode occurs (e.g. top left panel of Fig. 3 and Fig. 3 of M04). So, unless one mode just so happens to be completely “coupled” in the process of creating circular polarization, other propagation effects, such as the gyrotropy of the magnetospheric plasma, or cyclotron absorption (Melrose 2003) must be responsible for the production of circular polarization in the radio emission.

Karastergiou et al. (2003) and ES04 displayed the orientation angles of the polarization vector at a fixed pulse longitude using Hammer-Aitoff and Lambert equal-area projections. The colatitude and longitude histograms computed in §3 are simply another method for conveying the same information. Both the projections and the histograms effectively illustrate the fluctuations in the colatitude and longitude of the emission’s polarization vector.

A comprehensive version of the conditional density for the polarization vector’s orientation angles was derived. In its limiting forms, the conditional density follows the Watson bipolar distribution when the polarization amplitude is small ($\mu = \gamma = 0$) and follows the Fisher distribution when the polarization fluctuations are small compared to the effective noise ($\rho \ll 1$). Since both the Watson and Fisher distributions have many applications in the statistical analysis of scientific data (M03), the comprehensive version of the conditional density given by equation 8 may have more widespread applications.

The small values of polarization signal-to-noise ratio found in the orientation angle analysis and the inflated Q-U-V data point clusters found by M04 and ES04 are reminders that the effective noise of single pulse, polarization observations is much larger than the noise measured off the pulse. The additional noise may be due to RPR. The colatitude distribution (eqn. 6) was derived assuming Gaussian fluctuations in mode polarization amplitudes, and it is remarkable that the equation fits the data so well, regardless of the actual type of pulsar-intrinsic polarization fluctuations. Perhaps the good match between equation and data can be attributed to the idea that the observed fluctuations are heavily influenced by the large, effective Gaussian noise. The caution to interject here is that we are sifting through a large effective noise component in analyzing these data, irrespective of how low the off-pulse noise might be. Consequently, it is important to account for the effective noise in statistical models so that the data can be properly interpreted.

Again, I am indebted to Dan Stinebring for his continued generosity in providing the data used in the analysis. I thank an anonymous referee for comments that improved the manuscript.

REFERENCES

- Allen, M. C. & Melrose, D. B. 1982, *Proc. Astron. Soc. Aust.*, 4, 365
- Barnard, J. J. & Arons, J. 1986, *ApJ*, 302, 138
- Cordes, J. M., Rankin, J. M., & Backer, D. C. 1978, *ApJ*, 223, 961
- Edwards, R. T. & Stappers, B. W. 2004, *A&A*, 421, 681 (ES04)
- Fisher, N. I, Lewis, T., & Embleton, B. J. J. 1987, *Statistical Analysis of Spherical Data*, (Cambridge: Cambridge)
- Karastergiou, A., Johnston, S., & Kramer, M. 2003, *A&A*, 404, 325
- Lyubarskii, Y. E. & Petrova, S. A., 1998, *Ap&SS*, 262, 379
- Manchester, R. N., Taylor, J. H., & Huguenin, G. R. 1975, *ApJ*, 196, 83
- Melrose, D. B. 2003, in *ASP Conf. Ser. 302, Radio Pulsars*, ed. M. Bailes, D. J. Nice, & S. E. Thorsett (San Francisco: ASP), 179
- McKinnon, M. M. 2003, *ApJS*, 148, 519 (M03)
- McKinnon, M. M. 2004, *ApJ*, 606, 1154 (M04)
- McKinnon, M. M. & Stinebring, D. R. 1998, *ApJ*, 502, 883
- McKinnon, M. M. & Stinebring, D. R. 2000, *ApJ*, 529, 435
- Morris, D., Graham, D. A., & Sieber, W. 1981, *A&A*, 100, 107
- Petrova, S. A. 2001, *A&A*, 378, 883
- Stinebring, D. R., Cordes, J. M., Rankin, J. M., Weisberg, J. M., & Boriakoff, V. 1984, *ApJS*, 55, 247